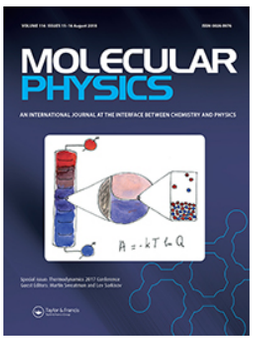

Taylor & Francis
Taylor & Francis Group

Molecular Physics

An International Journal at the Interface Between Chemistry and Physics

ISSN: 0026-8976 (Print) 1362-3028 (Online) Journal homepage: https://www.tandfonline.com/loi/tmph20

Equation of state for the Lennard-Jones truncated and shifted fluid with a cut-off radius of 2.5 σ based on perturbation theory and its applications to interfacial thermodynamics

Michaela Heier, Simon Stephan, Jinlu Liu, Walter G. Chapman, Hans Hasse & Kai Langenbach

To cite this article: Michaela Heier, Simon Stephan, Jinlu Liu, Walter G. Chapman, Hans Hasse & Kai Langenbach (2018) Equation of state for the Lennard-Jones truncated and shifted fluid with a cut-off radius of 2.5σ based on perturbation theory and its applications to interfacial thermodynamics, Molecular Physics, 116:15-16, 2083-2094, DOI: 10.1080/00268976.2018.1447153

To link to this article: https://doi.org/10.1080/00268976.2018.1447153

MOLECULAR PHYSICS
2018, VOL. 116, NOS. 15–16, 2083–2094
https://doi.org/10.1080/00268976.2018.1447153

Taylor & Francis
Taylor & Francis Group

THERMODYNAMICS 2017

Equation of state for the Lennard-Jones truncated and shifted fluid with a cut-off radius of 2.5 σ based on perturbation theory and its applications to interfacial thermodynamics

Michaela Heier [a], Simon Stephan [a], Jinlu Liu [b], Walter G. Chapman [b], Hans Hasse [a] and Kai Langenbach [a,b]

[a]Laboratory of Engineering Thermodynamics, University of Kaiserslautern, Kaiserslautern, Germany; [b]Chemical and Biomolecular Engineering Department, Rice University, Houston, TX, USA

ABSTRACT

An equation of state is presented for describing thermodynamic properties of the Lennard-Jones truncated and shifted (LJTS) potential with a cut-off radius of 2.5 σ. It is developed using perturbation theory with a hard-sphere reference term and labelled with the acronym PeTS (perturbed truncated and shifted). The PeTS equation of state describes the properties of the bulk liquid and vapour and the corresponding equilibrium of the LJTS fluid well. Furthermore, it is developed so that it can be used safely in the entire metastable and unstable region, which is an advantage compared to existing LJTS equations of state. This makes the PeTS equation of state an interesting candidate for studies of interfacial properties. The PeTS equation of state is applied here in two theories of interfaces, namely density gradient theory (DGT) and density functional theory (DFT). The influence parameter of DGT as well as the interaction averaging diameter of DFT are fitted to data of the surface tension of the LJTS fluid obtained from molecular simulation. The results from both theories agree very well with those from the molecular simulations.

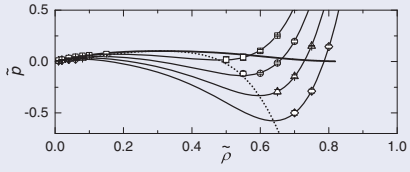

ARTICLE HISTORY
Received 1 December 2017
Accepted 22 February 2018

KEYWORDS
Equation of state; Lennard-Jones truncated and shifted; molecular dynamics simulation; density gradient theory; density functional theory

1. Introduction

The Lennard-Jones truncated and shifted (LJTS) potential with a cut-off radius of 2.5 σ is probably the cheapest intermolecular potential in terms of required computational effort that still gives a reasonable picture of the physics of simple fluids. Therefore, it is often used as a model fluid for studies of physical effects or for the development of methods in molecular simulations [1–15]. Molecular simulations are also often used to develop or test theories of the liquid state [16–18].

The standard Lennard-Jones (LJ) potential is

$$u_{\mathrm{LJ}}(r) = 4\varepsilon\left[\left(\frac{\sigma}{r}\right)^{12} - \left(\frac{\sigma}{r}\right)^{6}\right] \tag{1}$$

with ε and σ being the energy and size parameter, and r the distance between two particles. After truncation at the cut-off radius r_c and the shifting of the potential, the LJTS potential is obtained [19]:

$$u_{\mathrm{LJTS}}(r) = \begin{cases} u_{\mathrm{LJ}}(r) - u_{\mathrm{LJ}}(r_c) & r \le r_c \\ 0 & r > r_c \end{cases}. \tag{2}$$

In the present work r_c is 2.5 σ throughout. For brevity, we refer to that potential simply as LJTS in the following, without specifying r_c.

Lately, there has been a surge of interest in vapour–liquid interfaces, namely concerning microscopic details of their structure, e.g. [20–31]. Unfortunately, that structure cannot be studied by experiments due to the small length scale and its fluctuations. Hence, only theoretical studies and computer simulations are possible. The LJTS potential is an interesting candidate for such studies. In fact, it has been used before in many molecular simulation studies of interfaces, e.g. [4–6,8,9,11,16,32]. It is desirable to compare the results obtained from such studies to results obtained from theories of interfaces, namely

CONTACT Kai Langenbach Kai.Langenbach@mv.uni-kl.de

density gradient theory (DGT) and density functional theory (DFT). However, the basic requirement for such a comparison is that the equation of state (EOS) that is used in the interfacial theory is consistent with the potential used in the simulations, not only in the stable region but also in the metastable region [27,29,33–36], and that the EOS shows no unphysical behaviour in the metastable and unstable region.

There are many EOS for the LJ fluid [37–42], however these cannot be used for the LJTS fluid. For the LJTS fluid only two EOS are presently available [38,43]. Both do not fulfil the requirements described above. Johnson *et al.* [38] describe a method to transfer an EOS for the full LJ fluid to the LJTS fluid. Their method works reasonably well for cut-off radii above $3\,\sigma$, but for small cut-off radii, like the one used here, unphysical behaviour emerges. The EOS of Thol *et al.* [43] for the LJTS with $r_c = 2.5\,\sigma$ is essentially a correlation of the free energy with parameters fitted to a variety of properties and states. In the stable region this EOS performs very well, but it shows several van der Waals loops in the metastable and unstable region.

The development of the perturbed truncated and shifted (PeTS) EOS for the LJTS fluid is based on the perturbation theory of Barker and Henderson [44] assuming that the repulsion can be characterised by a hard-sphere term with a temperature-dependent segment diameter. The attraction is modelled by a series expansion of the first- and second-order perturbation integrals [44] similar to the work of Gross and Sadowski [45,46], who showed that on this basis good results are obtained. The series expansion contains adjustable parameters which are fitted to the vapour–liquid equilibrium (VLE) data of the LJTS fluid taken from Vrabec *et al.* [32], who have also given a comprehensive discussion of other simulation data on the LJTS fluid. The procedure described above results in the PeTS EOS, which is validated here in the stable and metastable region by a comparison with molecular simulation data obtained in the present work. The PeTS EOS shows good agreement with the simulation data and no unphysical behaviour beyond the spinodal. A comparison of PeTS EOS with literature data in the stable region [43] shows good agreement as well. In summary, it is shown that PeTS EOS is an accurate EOS for the LJTS fluid with $r_c = 2.5\,\sigma$, valid in the stable, metastable, and most likely also in the unstable region.

The PeTS EOS is applied in two interfacial theories, namely DGT and DFT. In DGT, the free energy of the heterogeneous system is developed around the free energy of the homogeneous system, i.e. the EOS, in terms of a gradient expansion [34–36]. In DFT for simple atomic fluids usually the theoretically derived fundamental measure theory (FMT) for repulsion [47–49] is used, while different approaches exist for treating the dispersion, e.g. [50–52]. FMT can be chosen such that the repulsive contribution of the EOS is reproduced in the homogeneous limit. In order to arrive at a functional with the same property for the dispersion term, the weighted density approximation (WDA) has turned out to be the best alternative [52]. This approach is used here. The functional derived in this way from PeTS EOS is termed PeTS-interfacial (PeTS-i). The influence parameter of DGT and the interaction averaging diameter of the WDA have to be fitted. Usually data on the surface tension is used for that purpose. Molecular simulation data on the surface tension of the LJTS fluid taken from [32] is used here for both DFT and DGT. The interaction averaging diameter of the WDA is fitted to the surface tension data at $\tilde{T} = 0.8$. The influence parameter of DGT is found to be independent of temperature within error bars. Both approaches are compared to thermodynamic data of the interface from simulation [32]. The agreement is almost perfect for both theories.

Throughout the paper, LJ-reduced units are used, cf. A.3. We treat molecular simulation throughout this article as reference data, so the concepts and methods applied here are straightforward to extend to real fluids.

2. Perturbed truncated and shifted (PeTS) equation of state

2.1. Development

The perturbation theory of Barker and Henderson [44] splits the residual free energy $\tilde{a}^{\mathrm{res}}$ into the free energy of a reference potential $\tilde{a}^{\mathrm{ref}}$ and a part due to the perturbation $\tilde{a}^{\mathrm{pert}}$

$$\tilde{a}^{\mathrm{res}} \equiv \tilde{a} - \tilde{a}^{\mathrm{id}} = \tilde{a}^{\mathrm{ref}} + \tilde{a}^{\mathrm{pert}} \tag{3}$$

where $\tilde{a}$ is the free energy per particle and $\tilde{a}^{\mathrm{id}}$ is the free energy per particle of the ideal gas. The LJTS potential is discretised with the modified step-square-well potential proposed by Chen and Kreglewski [53]:

$$\tilde{u}\left(\tilde{r}\right) = \begin{cases} \infty & \tilde{r} < (1 - c_1) \\ c_2 & (1 - c_1) \le \tilde{r} < 1 \\ -1 & 1 \le \tilde{r} < \lambda \\ 0 & \tilde{r} \ge \lambda \end{cases} \tag{4}$$

which has three parameters: c_1 and c_2 which characterise the repulsive part, and λ which characterises the attractive part. Only the repulsive part of the potential is used in the following, i.e. the paramter λ is not used. The attraction is handled implicitly as detailed below.

Using the approach of Barker and Henderson [44], the repulsive part of a potential can be described by an effective hard-sphere diameter $\tilde{d}$:

$$\tilde{d}(T) = \int_0^1 \left(1 - \exp\left(-\frac{\tilde{u}(\tilde{r})}{\tilde{T}}\right)\right) \mathrm{d}\tilde{r}. \tag{5}$$

Applied to the potential (4), this yields

$$\tilde{d}\left(\tilde{T}\right) = 1 - c_1 \exp\left(-\frac{c_2}{\tilde{T}}\right). \tag{6}$$

Following this approach, the reference term in Equation (3) is the free energy of the hard sphere which is according to Boublík [54] and Mansoori [55]:

$$\frac{\tilde{a}^{\mathrm{ref}}}{\tilde{T}} = \frac{\tilde{a}^{\mathrm{hs}}}{\tilde{T}} = \frac{3\eta}{1-\eta} + \frac{\eta}{(1-\eta)^2} \tag{7}$$

where η is the reduced packing fraction

$$\eta = \frac{\pi}{6}\tilde{\rho}\tilde{d}^3 \tag{8}$$

and $\tilde{\rho}$ is the number density. According to Barker and Henderson [44], the perturbation contribution in Equation (3), which describes only dispersion here, is

$$\frac{\tilde{a}^{\mathrm{pert}}}{\tilde{T}} = \frac{\tilde{a}_1}{\tilde{T}} + \frac{\tilde{a}_2}{\tilde{T}} \tag{9}$$

up to second order, where $\tilde{a}_1$ is the first-order dispersion contribution and $\tilde{a}_2$ the second-order dispersion contribution. These contributions are given by [45]

$$\frac{\tilde{a}_1}{\tilde{T}} = -2\pi\tilde{\rho}\frac{1}{\tilde{T}}\underbrace{\int_1^\infty \tilde{u}(\tilde{r}) f\left(\frac{\tilde{r}}{\tilde{d}}\right)\tilde{r}^2 \mathrm{d}\tilde{r}}_{I_1} \tag{10}$$

and

$$\frac{\tilde{a}_2}{\tilde{T}} = -\pi\tilde{\rho}\left(1 + \frac{8\eta - 2\eta^2}{(1-\eta)^4}\right)^{-1} \times \left(\frac{1}{\tilde{T}}\right)^2 \underbrace{\frac{\partial}{\partial\tilde{\rho}}\left[\int_1^\infty \tilde{u}(\tilde{r})^2 f\left(\frac{\tilde{r}}{\tilde{d}}\right)\tilde{r}^2 \mathrm{d}\tilde{r}\right]}_{I_2}. \tag{11}$$

In analogy to the approach of Gross and Sadowski [45], the integrals I_1 and I_2 in Equations (10) and (11) are developed into a Taylor series as functions of the packing fraction only

$$I_1 = \sum_{i=0}^{6} a_i \eta^i \tag{12}$$

$$I_2 = \sum_{i=0}^{6} b_i \eta^i \tag{13}$$

for which 14 state-independent parameters are used: a_i and b_i with $i \in \{0, 1, 2, 3, 4, 5, 6\}$. Additionally, the parameters c_1 and c_2 that characterise the repulsive part of the potential (4) have to be determined.

2.2. Parameterisation

The resulting 16 parameters were fitted to saturated liquid and vapour densities $\tilde{\rho}^{\mathrm{l}}$ and $\tilde{\rho}^{\mathrm{v}}$ and vapour pressures $\tilde{p}^{\mathrm{s}}$ of the LJTS fluid for temperatures $\tilde{T}$ between 0.64 and 1.06. The data was taken from Vrabec *et al.* [32]. The data from the metastable region presented in this article was not used for fitting. The resulting parameters are given in Table 1. The objective function S used in the fit was

$$S = \sum_{\Omega} s_\Omega \tag{14}$$

with

$$s_\Omega = \frac{\sqrt{\sum_{m=1}^{M}\left(\frac{\Omega_{m,\mathrm{MD}} - \Omega_{m,\mathrm{EOS}}}{\Omega_{m,\mathrm{MD}}}\right)^2}}{M} \tag{15}$$

Table 1. Parameters of the PeTS EOS and DGT influence parameter.

Parameter	Value	Parameter	Value	Parameter	Value
a_0	0.690603404	b_0	0.664852128	c_1	0.127112544
a_1	1.189317012	b_1	2.10733079	c_2	3.052785558
a_2	1.265604153	b_2	−9.597951213		
a_3	−24.34554201	b_3	−17.37871193	$\tilde{\kappa}_{\mathrm{PeTS}}$	2.7334
a_4	93.67300357	b_4	30.17506222		
a_5	−157.8773415	b_5	209.3942909		
a_6	96.93736697	b_6	−353.2743581		

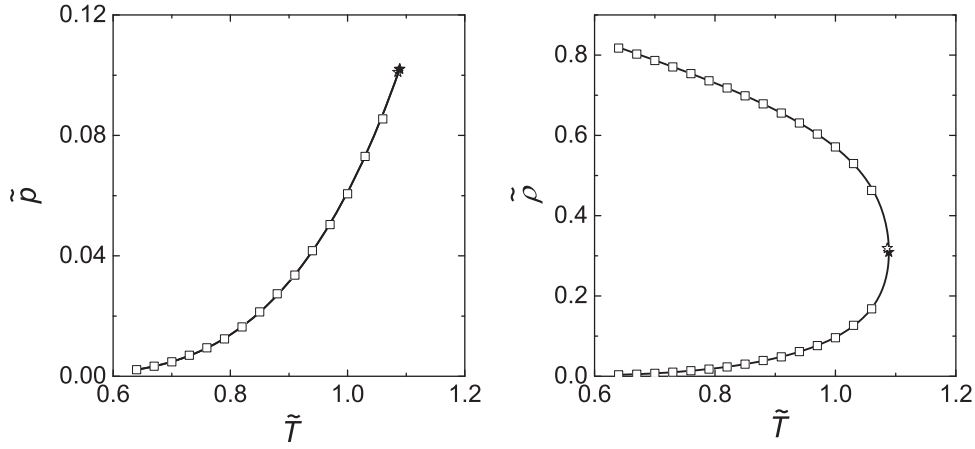

Figure 1. Vapour pressure curve (left) and saturated densities (right) of the LJTS fluid obtained with the PeTS EOS (line) and with molecular simulation [32] (squares).

where M is the number of data points, Ω stands for either $\tilde{\rho}^{\mathrm{l}}$, $\tilde{\rho}^{\mathrm{v}}$ or $\tilde{p}^{\mathrm{s}}$ and the subscripts MD and EOS refer to the simulation data from [32] or the results from the EOS, respectively. The final sums of squares for the three state variables are $s_{\tilde{\rho}^{\mathrm{l}}} = 0.00026$, $s_{\tilde{\rho}^{\mathrm{v}}} = 0.00330$ and $s_{\tilde{p}^{\mathrm{s}}} = 0.00265$.

In Figure 1, the results of the PeTS EOS (solid lines) and the VLE data of Vrabec *et al.* [32] (squares) are compared. The results from the PeTS EOS are in very good agreement with the simulation data. This can also be seen in Figure 2, where the deviation of the results calculated with the PeTS EOS from the simulation data by Vrabec *et al.* [32] is displayed. Figure 2 also includes the deviation of the results from the EOS of Thol *et al.* [43] from the simulation data. In most cases, the deviations do not exceed the statistical uncertainty of the simulation data. This holds for both EOS.

2.3. Comparison to computer experiments

2.3.1. Stable states

Thol *et al.* [43] report simulation data for the pressure as a function of temperature and density for homogeneous stable states for a wide range of conditions. That data, even though it was not included in the present fit, is represented well by the PeTS EOS, cf. Figure 3. For given temperature and density, the relative deviation in the pressure is in most cases below 5%. Three simulation data points of Thol *et al.* [43] are not included in Figure 3. They show very high deviations from both the PeTS EOS and the EOS of Thol *et al.* [43] and are probably erroneous.

The EOS of Thol *et al.* [43] describes the simulation data, to which it was fitted, better than the PeTS EOS. Still the predictions of the PeTS EOS for that data are good.

2.3.2. Metastable states

Simulations of metastable states are carried out in the present work with two different techniques yielding $p - \rho - T$ data or $\mu - p - T$ data, respectively. The simulation techniques are explained in A.1 and A.2. Besides data in the metastable region, also some data points in the stable region were obtained with these methods. The results of the computer experiments are compared to the results of the PeTS EOS and to those of the EOS of Thol *et al.* [43] in Figure 4. Besides the overall picture (left), Figure 4 also contains a zoomed plot of the gas side (right). The binodal as obtained from the PeTS EOS does not differ significantly from that obtained from the EOS of Thol *et al.* [43]. The error bars of the simulation results are mostly within symbol size. Only close to the spinodal on the liquid side of the phase equilibrium the error bars are relatively large due to low particle numbers in these simulations. While in the homogeneous region both EOS perform equally well, there are important differences in the metastable region. The subcritical isotherms of the EOS of Thol *et al.* [43] have two minima and two maxima whereas those from the PeTS EOS have only one minimum and one maximum, so that only the latter can be used together with DGT for studying properties of fluid interfaces. Also, the spinodals found from both EOS differ significantly. The metastable region predicted by the EOS of Thol *et al.* [43] is significantly smaller than that predicted by the PeTS EOS, i.e. the spinodal predicted by the EOS of Thol *et al.* [43] encloses four of the state points for which simulation results were obtained here, thereby erroneously predicting instability. The simulation data obtained here for the metastable region confirms the results of the PeTS EOS.

In Figure 5, results of the PeTS EOS (line) and the simulations (symbols) of $\mu - p - T$ behaviour are

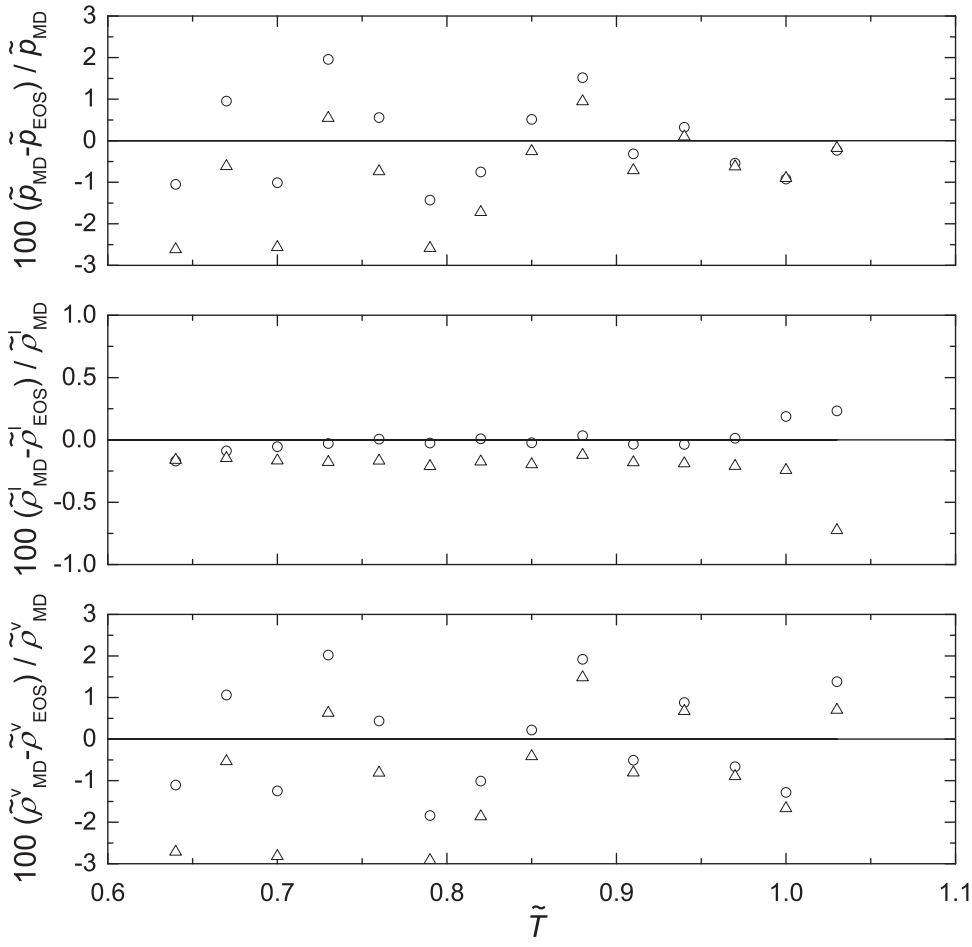

Figure 2. Deviations of results obtained with the PeTS EOS (circles) and the EOS from Thol *et al*. [43] (triangles) from molecular simulation data of Vrabec *et al*. [32] for the vapour pressure (top), saturated liquid density (middle) and saturated vapour density (bottom) of the LJTS fluid.

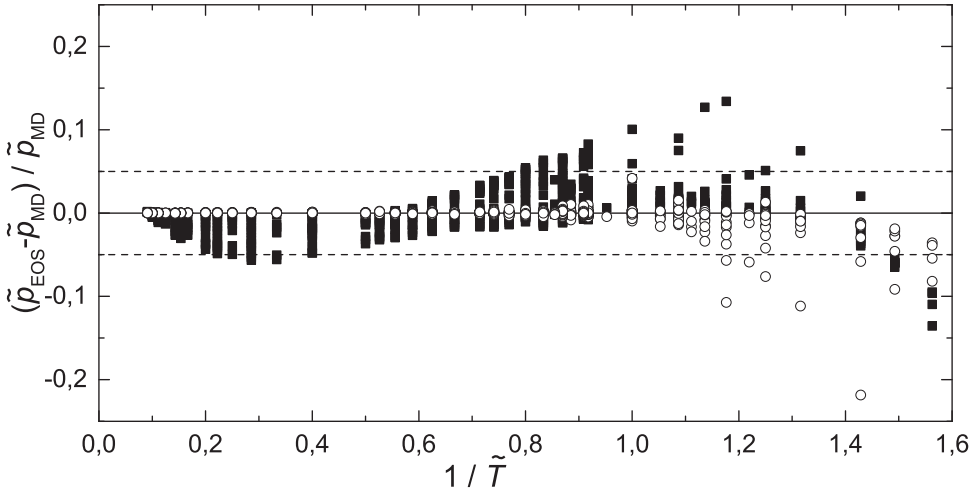

Figure 3. Deviation of results for the pressure obtained with the PeTS EOS (full squares) and the EOS of Thol *et al*. [43] (open circles) from the simulation data of homogeneous states of the LJTS fluid [43]. All states given by Thol *et al*. [43] are used for the comparison except for three state points as described in the text. The dashed lines show the deviation of ±5%.

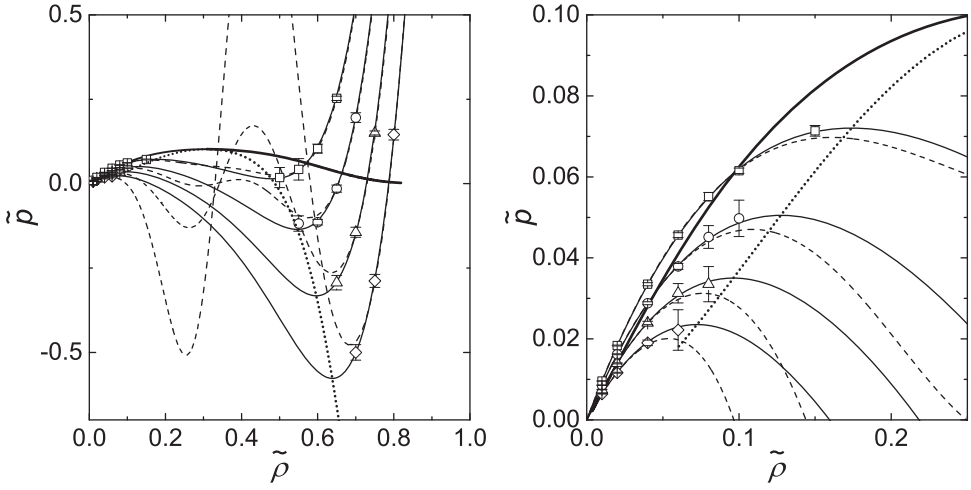

Figure 4. Thermal properties of the LJTS fluid: isotherms obtained with the PeTS EOS (solid line), the EOS of Thol *et al*. [43] (dashed line) and from MD simulations for $\tilde{T} = 1.0$ (squares), $\tilde{T} = 0.9$ (circles), $\tilde{T} = 0.8$ (triangles) and $\tilde{T} = 0.7$ (diamonds). The thick solid line is the binodal and the dotted line is the spinodal from the PeTS EOS. The binodal from the EOS of Thol *et al*. [43] is practically identical with the depicted one. The spinodal from the EOS of Thos *et al*. [43] is not shown for clarity, but differs significantly.

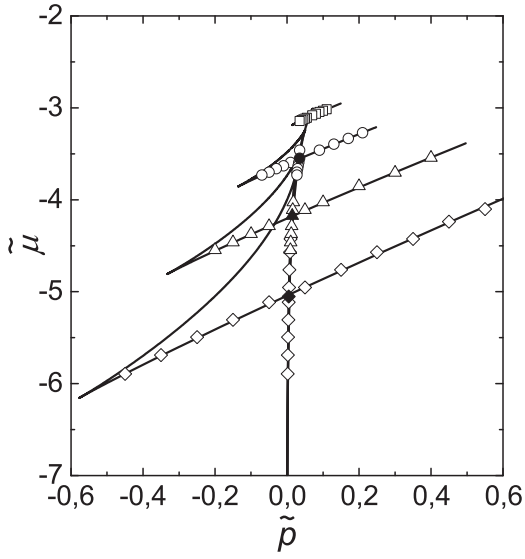

Figure 5. Chemical potential of the LJTS fluid as a function of pressure obtained from the PeTS EOS (lines) and from molecular simulations (symbols) for $\tilde{T} = 1.0$ (squares), $\tilde{T} = 0.9$ (circles), $\tilde{T} = 0.8$ (triangles) and $\tilde{T} = 0.7$ (diamonds). Vapour states are found on the steep branch in the middle and coincide for all temperatures. The almost straight flat branches correspond to liquid states and the curved branches, which can only be determined by the EOS, correspond to unstable states. VLE points are marked with filled symbols.

shown. In the $\mu - p$ projection of the phase space, equilibrium points are given by the self-intersection of the isotherm. Vapour states are found on the almost vertical part of the isotherm, where stable points are below the intersection and metastable points are above it. Liquid states are on the other linear branch of the isotherm, where pressures higher than that at the intersection indicate stable states and lower pressures indicate metastable states. Unstable states are found on the curved part of the isotherm connecting the vapour and liquid line. The latter can only be obtained from the PeTS EOS. Simulation data and results from PeTS EOS agree very well.

3. Application of PeTS EOS to vapour–liquid interfaces

The surface tension of the LJTS fluid is modelled here with two theoretical approaches, namely DGT and DFT and the results are compared to those from molecular simulations [32].

3.1. PeTS + density gradient theory

3.1.1. Structure

DGT describes the (static) change in density at interfaces by defining the free energy of the bulk fluid and the so-called influence parameter $\tilde{\kappa}$. A description of DGT is given by Miqueu *et al.* [56] who calculate the surface tension from

$$\tilde{\gamma} = \sqrt{2\tilde{\kappa}_{\mathrm{PeTS}}} \int_{\tilde{\rho}^{\mathrm{v}}}^{\tilde{\rho}^{\mathrm{l}}} \sqrt{\Delta\tilde{\omega}}\,\mathrm{d}\tilde{\rho} \tag{16}$$

where $\Delta\tilde{\omega}$ is the grand thermodynamic potential defined as $\Delta\tilde{\omega} = \tilde{\rho}\tilde{a}_0(\tilde{\rho}) - \tilde{\rho}\tilde{\mu}^{\mathrm{s}} + \tilde{p}^{\mathrm{s}}$. $\tilde{a}_0(\tilde{\rho})$ is the homogeneous

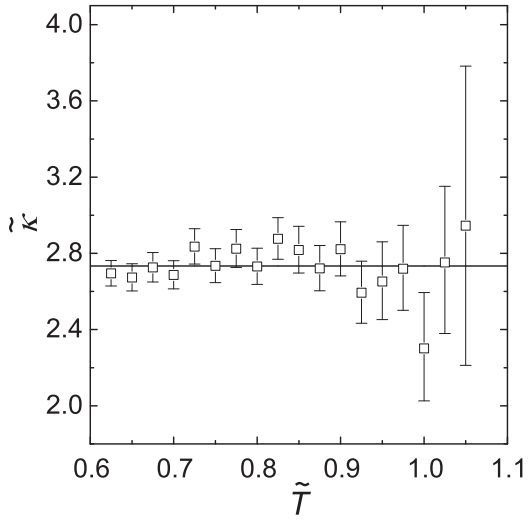

Figure 6. Influence parameter $\tilde{\kappa}$ of DGT calculated from molecular simulation data of the surface tension of the LJTS fluid [32]. The error bars are calculated from the surface tension error bars [32]. The horizontal line shows the chosen temperature-independent $\tilde{\kappa}_{\mathrm{PeTS}}$ value.

free energy per particle at the local density $\tilde{\rho}$, $\tilde{\mu}^{\mathrm{s}}$ is the saturated bulk phase chemical potential and $\tilde{p}^{\mathrm{s}}$ is the saturated bulk pressure.

3.1.2. Parameterisation

The influence parameter $\tilde{\kappa}$ for DGT is fitted here to surface tension data of the LJTS fluid obtained from molecular dynamics simulation [32]. First, each of the 18 data points for $\tilde{\gamma}_{\mathrm{MD}}(\tilde{T})$ provided by [32] is used to calculate the influence parameter individually. The results are shown as symbols in Figure 6. These $\tilde{\kappa}$ values reproduce the exact molecular simulation surface tension results. The error bars of the surface tension from molecular simulations, specified by Vrabec *et al.* [32], are transferred to error bars in $\tilde{\kappa}$, as shown in Figure 6. The horizontal line in Figure 6 is an error weighted average of the influence parameters with the value $\tilde{\kappa}_{\mathrm{PeTS}} = 2.7334$. This value is used in the following, since it is constant within error bars for all but one single simulation data point (cf. Figure 6).

3.2. PeTS + density functional theory

3.2.1. Structure

As in the EOS, the free energy is written in DFT as a sum of contributions:

$$\tilde{A}[\tilde{\rho}(\tilde{\mathbf{r}})] = \tilde{A}^{\mathrm{id}}[\tilde{\rho}(\tilde{\mathbf{r}})] + \tilde{A}^{\mathrm{hs}}[\tilde{\rho}(\tilde{\mathbf{r}})] + \tilde{A}^{\mathrm{pert}}[\tilde{\rho}(\tilde{\mathbf{r}})]. \quad (17)$$

where the squared brackets indicate a functional dependence on $\tilde{\rho}(\tilde{\mathbf{r}}_1)$.

In order to be consistent with PeTS, the white-bear version of FMT by Roth *et al.* [48] is used for $\tilde{A}^{\mathrm{hs}}[\tilde{\rho}(\tilde{\mathbf{r}})]$ that reduces to the Carnhan–Starling hard-sphere EOS in the bulk fluid. For the perturbation contribution the WDA

$$\tilde{A}^{\mathrm{pert}}[\tilde{\rho}(\tilde{\mathbf{r}})] = \int \overline{\tilde{\rho}}(\tilde{\mathbf{r}}_1)\tilde{a}^{\mathrm{pert}}(\overline{\tilde{\rho}}(\tilde{\mathbf{r}}_1))\mathrm{d}\tilde{\mathbf{r}}_1 \quad (18)$$

of Sauer and Gross [52] is used. We refer to Roth *et al.* [48], as well as Sauer and Gross [52] for details, also concerning the ideal gas term. In Equation (18), $\overline{\tilde{\rho}}$ is a weighted density at position $\tilde{\mathbf{r}}_1$

$$\overline{\tilde{\rho}}(\tilde{\mathbf{r}}_1) = \frac{3}{4\pi\,(\varphi\tilde{d})^3}\int \tilde{\rho}(\tilde{\mathbf{r}}_2)\Theta(\varphi\tilde{d} - |\tilde{\mathbf{r}}_1 - \tilde{\mathbf{r}}_2|)\mathrm{d}\tilde{\mathbf{r}}_2 \quad (19)$$

where a volume average within a sphere of diameter $\varphi\tilde{d}$, the interaction averaging diameter, is used for weighting, Θ is the Heaviside function and φ is an adjustable parameter which indicates the range of averaging. Density profiles are calculated as usual [57] by solving the Euler–Lagrange equation obtained from functional minimisation of the free energy. The surface tension of the planar interface is calculated from

$$\tilde{\gamma} = \int (\tilde{\rho}\tilde{a}[\tilde{\rho}(\tilde{z})] + \tilde{p}^{\mathrm{s}} - \tilde{\rho}(\tilde{z})\tilde{\mu}^{\mathrm{s}})\mathrm{d}\tilde{z} \quad (20)$$

where $\tilde{a}[\tilde{\rho}(\tilde{z})]$ is defined by Equation (17) and

$$\tilde{A}[\tilde{\rho}(\tilde{z})] = \tilde{S}\int \tilde{\rho}\tilde{a}[\tilde{\rho}(\tilde{z})]\mathrm{d}\tilde{z} \quad (21)$$

with $\tilde{S}$ being the area of the surface perpendicular to $\tilde{z}$. Numerical calculations are performed on a $20\,\sigma$ domain with finite $\Delta\tilde{z} = 0.01$.

3.2.2. Parameterisation

The parameter φ is obtained by fitting the calculated surface tension to the surface tension of Vrabec *et al.* [32] at $\tilde{T} = 0.8$. The fitted value is $\varphi = 1.21$.

3.3. Comparison to computer experiments

Figure 7 (top) shows the results of the surface tension $\tilde{\gamma}$ from DGT (solid line), DFT (triangles) and the molecular simulations [32] (squares) as a function of the temperature. Almost the entire range ($\tilde{T} = 0.65 \ldots 1.05$) between the triple point and the critical point is studied.

Since the error bars are within the symbol size in the top graph of Figure 7, the absolute deviation $\Delta\tilde{\gamma} = \tilde{\gamma}_{\mathrm{DGT/DFT}} - \tilde{\gamma}_{\mathrm{MD}}$ is shown in the lower graph of Figure 7. The surface tension values from DGT and DFT lie within

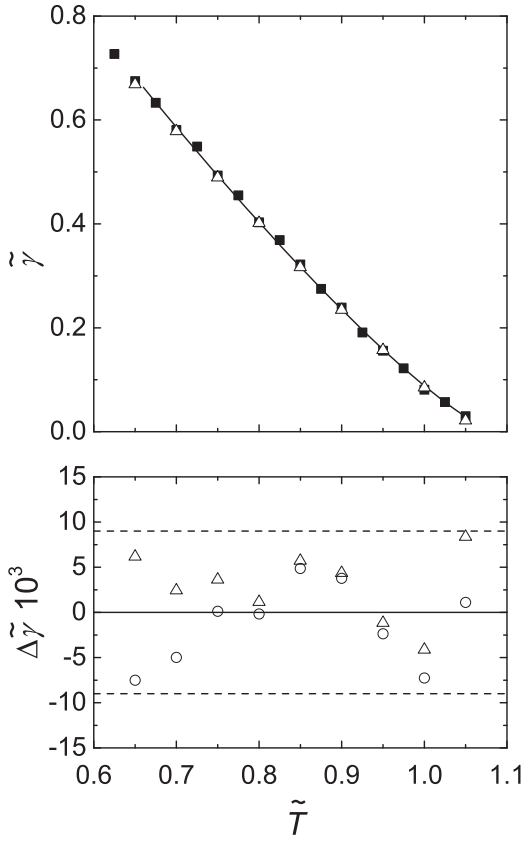

Figure 7. Top: surface tension of the LJTS fluid from molecular simulations (full squares) [32], DGT (line) and DFT (open triangles) as a function of the temperature. Simulation error bars are within the symbol size.
Bottom: absolute deviation of the surface tension results calculated by DGT (circles) and by DFT (triangles) from the molecular simulation results of [32] as function of temperature. The dotted lines indicate maximum error bars from molecular simulations.

the error bars of the simulation data in a broad temperature range.

We therefore conclude that a temperature-independent influence parameter for DGT is, at least in this case, adequate and the WDA [52] of DFT is accurate, if the parameter φ is fitted to only one data point.

4. Conclusions

The LJTS fluid with a cut-off radius of 2.5 σ is one of the computationally cheapest intermolecular potentials, but still gives a reasonable picture of the thermodynamics of simple fluids. It is therefore often used as a model fluid, namely for studying fluid interfaces by molecular simulations. Properties of interfaces can also be studied by DGT or DFT based on an EOS. EOS from the literature for the LJTS fluid [38,43] cannot be used in interfacial theories due to lacking accuracy [38] or unphysical behaviour in the unstable region [43]. In the present work, therefore, an EOS for the LJTS fluid was developed based on perturbation theory: the PeTS EOS. It gives similar results for the VLE as the best existing EOS for the LJTS fluid, that of Thol *et al.* [43], but shows no unphysical behaviour in the metastable or unstable region.

The PeTS EOS has a simple structure and was parameterised only to VLE data. That data is well described by the PeTS EOS. But PeTS EOS also predicts accurately molecular simulation results in the metastable region, as well as data on homogeneous stable states, including states far above the critical point. The PeTS EOS was applied in a DGT and a DFT approach for modelling the surface tension in VLE. The DGT influence parameter $\tilde{\kappa}$ is found to be constant within error bars of the molecular simulations data. The DFT interaction averaging diameter is only fit to one surface tension. The resulting surface tension of the LJTS fluid calculated by DGT and DFT lies within the error bars of the molecular simulation results.

The PeTS EOS can be extended easily to mixtures using mixing rules for its two parameters ε and σ and therefore lends itself to studies of fluid interfaces of mixtures in conjunction with DGT or DFT, which then can be compared directly to corresponding molecular simulations.

Acknowledgement

The authors gratefully acknowledge funding of the present work by Deutsche Forschungsgemeinschaft DFG within CRC926 and by European Research Council (ERC) under the European Union's Horizon 2020 research and innovation programme (grant agreement No. 694807 - ENRICO). The authors thank Philippe Ungerer and Martin Horsch for fruitful discussions. The present work was conducted under the auspices of the Boltzmann-Zuse Society of Computational Molecular Engineering (BZS) and the simulations were carried out on the Regional University Computing Center Kaiserslautern (RHRK) under the grant TUK-TLMV, the High Performance Computing Center Stuttgart (HLRS) under the grant MMHBF as well as the Leibniz Supercomputing Centre (LRZ) under the grant SPARLAMPE (pr48te).

Disclosure statement

No potential conflict of interest was reported by the authors.

Funding

Deutsche Forschungsgemeinschaft (DFG) [grant number CRC926]; European Research Council under the European Union's Horizon 2020 [grant number 694807 - ENRICO]; Regional University Computing Center Kaiserslautern (RHRK) [grant TUK-TLMV]; High Performance Computing Center

Stuttgart (HLRS) [grant MMHBF]; Leibniz Supercomputing Centre (LRZ) [grant SPARLAMPE (pr48te)].

ORCID

Michaela Heier http://orcid.org/0000-0003-3950-1606
Kai Langenbach http://orcid.org/0000-0001-5025-6360

References

[1] A.I. Rusanov and E.N. Brodskaya, J. Colloid Interface Sci. **62**(3), 542 (1977). doi:10.1016/0021-9797(77)90105-9
[2] E.S. Landry, S. Mikkilineni, M. Paharia, and A.J.H. McGaughey, J. Appl. Phys. **102**(12), 124301 (2007). doi:10.1063/1.2821753
[3] T. Kraska, J. Phys. Chem. B **112**(39), 12408 (2008). doi:10.1021/jp806315e
[4] M. Horsch, H. Hasse, A.K. Shchekin, A. Agarwal, S. Eckelsbach, J. Vrabec, E.A. Müller, and G. Jackson, Phys. Rev. E **85**(3), 031605 (2012). doi:10.1103/PhysRevE.85.031605
[5] A. Lotfi, J. Vrabec, and J. Fischer, Int. J. Heat Mass Transfer **73**, 303 (2014). doi:10.1016/j.ijheatmasstransfer.2014.02.010
[6] S. Becker, H.M. Urbassek, M. Horsch, and H. Hasse, Langmuir **30**(45), 13606 (2014). doi:10.1021/la503974z
[7] J.J. Derksen, AIChE J. **61**(11), 4020 (2015). doi:10.1002/aic.14930
[8] M. Heinen, J. Vrabec, and J. Fischer, J. Chem. Phys. **145**(8), 081101 (2016). doi:10.1063/1.4961542
[9] M. Horsch, S. Miroshnichenko, and J. Vrabec, J. Phys. Stud. **13**(4), 4004 (2009).
[10] I. Napari, J. Julin, and H. Vehkamäki, J. Chem. Phys. **131**(24), 244511 (2009). doi:10.1063/1.3279127
[11] M. Horsch, M. Heitzig, C. Dan, J. Harting, H. Hasse, and J. Vrabec, Langmuir **26**(13), 10913 (2010). doi:10.1021/la1008363
[12] W. Eckhardt, A. Heinecke, R. Bader, M. Brehm, N. Hammer, H. Huber, H.G. Kleinhenz, J. Vrabec, H. Hasse, M. Horsch, M. Bernreuther, C.W. Glass, C. Niethammer, A. Bode, and H.J. Bungartz, 591 TFLOPS Multi-trillion Particles Simulation on SuperMUC. in *Supercomputing*, Lecture Notes in Computer Science, Jun. (Springer, Berlin, Heidelberg, 2013), pp. 1–12.
[13] S. Werth, S.V. Lishchuk, M. Horsch, and H. Hasse, Physica A **392**(10), 2359 (2013). doi:10.1016/j.physa. 2013.01.048
[14] C. Niethammer, S. Becker, M. Bernreuther, M. Buchholz, W. Eckhardt, A. Heinecke, S. Werth, H.J. Bungartz, C.W. Glass, H. Hasse, J. Vrabec, and M. Horsch, J. Chem. Theory Comput. **10**(10), 4455 (2014). doi:10.1021/ct500169q
[15] M. Horsch and H. Hasse, Chem. Eng. Sci. **107**, 235 (2014). doi:10.1016/j.ces.2013.12.026
[16] M. Horsch, J. Vrabec, and H. Hasse, Phys. Rev. E **78**(1), 011603 (2008). doi:10.1103/PhysRevE.78.011603
[17] I. Napari, J. Julin, and H. Vehkamäki, J. Chem. Phys. **133**(15), 154503 (2010). doi:10.1063/1.3502643
[18] R. Hołyst, M. Litniewski, and P. Garstecki, Phys. Rev. E **82**(6), 066309 (2010).
[19] M.P. Allen and D.J. Tildesley, *Computer Simulation of Liquids* (Oxford University Press, Oxford, 1989).
[20] E. Johannessen, J. Gross, and D. Bedeaux, J. Chem. Phys. **129**(18), 184703 (2008). doi:10.1063/1.3009182
[21] J. Gross, J. Chem. Phys. **131**(20), 204705 (2009). doi:10.1063/1.3263124
[22] O.G. Niño Amézquita, S. Enders, P.T. Jaeger, and R. Eggers, J. Supercrit. Fluids **55**(2), 724 (2010).
[23] X. Tang and J. Gross, J. Supercrit. Fluids **55**(2), 735 (2010). doi:10.1016/j.supflu.2010.09.041
[24] G. Niño-Amézquita, D. van Putten, and S. Enders, Fluid Phase Equilib. **332**, 40 (2012).
[25] E. Schäfer, G. Sadowski, and S. Enders, Fluid Phase Equilib. **362**, 151 (2014).
[26] C. Klink and J. Gross, Ind. Eng. Chem. Res. **53**(14), 6169 (2014). doi:10.1021/ie4029895
[27] A. Mejía, M. Cartes, H. Segura, and E.A. Müller, J. Chem. Eng. Data **59**(10), 2928 (2014).
[28] C. Cumicheo, M. Cartes, H. Segura, E.A. Müller, and A. Mejía, Fluid Phase Equilib. **380**, 82 (2014). doi:10.1016/j.fluid.2014.07.039
[29] S. Werth, M. Kohns, K. Langenbach, M. Heilig, M. Horsch, and H. Hasse, Fluid Phase Equilib. **427**, 219 (2016). doi:10.1016/j.fluid.2016.07.016
[30] S. Becker, S. Werth, M. Horsch, K. Langenbach, and H. Hasse, Fluid Phase Equilib. **427**, 476 (2016). doi:10.1016/j.fluid.2016.08.007
[31] J. Mairhofer and J. Gross, Fluid Phase Equilib. **439**, 31 (2017). doi:10.1016/j.fluid.2017.02.009
[32] J. Vrabec, G.K. Kedia, G. Fuchs, and H. Hasse, Mol. Phys. **104**(9), 1509 (2006). doi:10.1080/00268970600556774
[33] A. Keller, K. Langenbach, and H. Hasse, Fluid Phase Equilib. **444**, 31 (2017). doi:10.1016/j.fluid.2017.04.009
[34] J.D. van der Waals, Ph. D. thesis, Leiden University, 1873.
[35] J.W. Cahn and J.E. Hilliard, J. Chem. Phys. **28**(2), 258 (1958). doi:10.1063/1.1744102
[36] J.W. Cahn, J. Chem. Phys. **30**(5), 1121 (1959). doi:10.1063/1.1730145
[37] J.J. Nicolas, K.E. Gubbins, W.B. Streett, and D.J. Tildesley, Mol. Phys. **37**(5), 1429 (1979). doi:10.1080/00268977900101051
[38] J.K. Johnson, J.A. Zollweg, and K.E. Gubbins, Mol. Phys. **78**(3), 591 (1993). doi:10.1080/00268979300100411
[39] J. Kolafa and I. Nezbeda, Fluid Phase Equilib. **100**, 1 (1994). doi:10.1016/0378-3812(94)80001-4
[40] M. Mecke, A. Müller, J. Winkelmann, J. Vrabec, J. Fischer, R. Span, and W. Wagner, Int. J. Thermophys. **17**(2), 391 (1996). doi:10.1007/BF01443399
[41] H.O. May and P. Mausbach, Phys. Rev. E **85**(3), 031201 (2012). doi:10.1103/PhysRevE.85.031201
[42] M. Mecke, A. Müller, J. Winkelmann, and J. Fischer, Int. J. Thermophys. **18**(3), 683 (1997). doi:10.1007/BF02575128
[43] M. Thol, G. Rutkai, R. Span, J. Vrabec, and R. Lustig, Int. J. Thermophys. **36**(1), 25 (2015). doi:10.1007/s10765-014-1764-4
[44] J.A. Barker and D. Henderson, J. Chem. Phys. **47**(11), 4714 (1967). doi:10.1063/1.1701689
[45] J. Gross and G. Sadowski, Ind. Eng. Chem. Res. **40**(4), 1244 (2001). doi:10.1021/ie0003887
[46] J. Gross and G. Sadowski, Fluid Phase Equilib. **168**(2), 183 (2000). doi:10.1016/S0378-3812(00)00302-2
[47] Y. Rosenfeld, Phys. Rev. Lett. **63**(9), 980 (1989). doi:10.1103/PhysRevLett.63.980
[48] R. Roth, R. Evans, A. Lang, and G. Kahl, J. Phys.: Condens. Matter **14**(46), 12063 (2002). doi:10.1088/0953-8984/14/46/313

[49] Y.X. Yu and J. Wu, J. Chem. Phys. **117**(22), 10156 (2002). doi:10.1063/1.1520530
[50] S. Tripathi and W.G. Chapman, Phys. Rev. Lett. **94**(8), 087801 (2005). doi:10.1103/PhysRevLett.94.087801
[51] B.D. Marshall and W.G. Chapman, J. Phys. Chem. B **115**(50), 15036 (2011). doi:10.1021/jp2078677
[52] E. Sauer and J. Gross, Ind. Eng. Chem. Res. **56**(14), 4119 (2017). doi:10.1021/acs.iecr.6b04551
[53] S.S. Chen and A. Kreglewski, Ber. Bunsen-Ges. Phys. Chem. **81**(10), 1048 (1977). doi:10.1002/bbpc.19770811037
[54] T. Boublík, J. Chem. Phys. **53**(1), 471 (1970).
[55] G.A. Mansoori, N.F. Carnahan, K.E. Starling, and T.W. Leland, J. Chem. Phys. **54**(4), 1523 (1971). doi:10.1063/1.1675048
[56] C. Miqueu, B. Mendiboure, A. Graciaa, and J. Lachaise, Fluid Phase Equilib. **207**(1), 225 (2003). doi:10.1016/S0378-3812(03)00028-1
[57] S. Tripathi and W.G. Chapman, J. Chem. Phys. **122**(9), 094506 (2005). doi:10.1063/1.1853371
[58] C.W. Glass, S. Reiser, G. Rutkai, S. Deublein, A. Köster, G. Guevara-Carrion, A. Wafai, M. Horsch, M. Bernreuther, T. Windmann, H. Hasse, and J. Vrabec, Comput. Phys. Commun. **185**(12), 3302 (2014). doi:10.1016/j.cpc.2014.07.012
[59] B. Widom, J. Chem. Phys. **39**(11), 2808 (1963). doi:10.1063/1.1734110
[60] H.C. Andersen, , J. Chem. Phys. **72**(4), 2384 (1980). doi:10.1063/1.439486
61 G. Rutkai, A. Köster, G. Guevara-Carrion, T. Janzen, M. Schappals, C.W. Glass, M. Bernreuther, A. Wafai, S. Stephan, M. Kohns, S. Reiser, S. Deublein, M. Horsch, H. Hasse, and J. Vrabec, Comput. Phys. Commun., **221**, 343 (2017). doi:10.1016/j.cpc.2017.07.025

Appendix. *Computer experiments*

A1. p − ρ − T Simulations

Molecular dynamics (MD) simulations of stable and metastable states of the LJTS fluid are carried out in the canonical (*NVT*) ensemble using *ls1 mardyn* [14]. For four isotherms ($\tilde{T} = 0.7, 0.8, 0.9, 1.0$) the pressure is determined as a function of the density. The temperature is kept constant with velocity scaling. The number of particles varies from 864 to 50 as indicated in Table A1 for reasons given below. The time step is $\Delta\tilde{t} = 0.0005$. The simulations are carried out for at least 2,000,000 time steps. The mean bulk pressure is determined from the last 1,000,000 time steps. The statistical error of the results is estimated as three times the standard deviation of five block averages where the block length is 200,000 time steps.

By reducing the volume of the simulation box and the number of particles for simulations near the spinodal (cf. Table A1) the probability of a homogeneous nucleation event is reduced so that simulations without nucleation can be carried out for a sufficiently long time to get a good sampling. Simulations in which nucleation events occur are discarded. Bubble nucleation is detected by a kink in the pressure–density relation. Droplet nucleation is detected by a sudden rise in pressure fluctuations typical for liquid phases as described in [33]. On the vapour side the lowest number of particles is 50. On the liquid side it is 200. The larger number of particles on the liquid side is necessary because otherwise the last maximum of the radial distribution function $g(\tilde{r})$ would be truncated, such that finite size effects would occur.

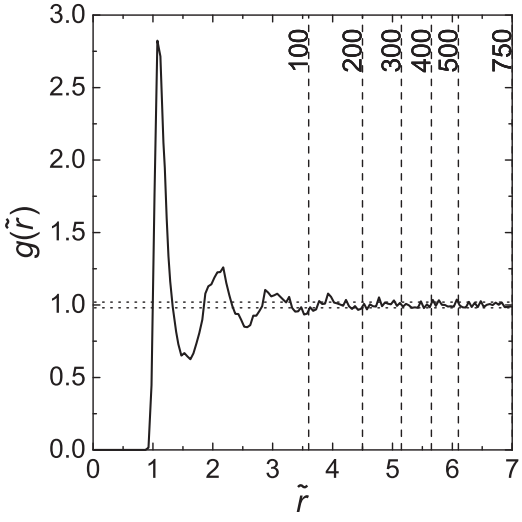

Figure A1. Radial distribution function of the LJTS fluid for $\tilde{T} = 0.7$, $\tilde{\rho} = 0.787$ and $N = 1000$ particles. The two horizontal dotted lines display the standard deviation of $g(\tilde{r})$ for large values of $\tilde{r}$. The dashed lines show the truncation of the radial distribution functions for $N = 100$, $N = 200$, $N = 300$, $N = 400$, $N = 500$ and $N = 750$.

Figure A1 shows the radial distribution function of the saturated LJTS fluid at $\tilde{T} = 0.7$ obtained from a simulation with 1000 particles. The dashed lines show the truncations of the radial distribution functions for smaller numbers of particles due to the finite box size whereas the dotted lines show the standard deviation of $g(\tilde{r}) = 1.0$ for large values of $\tilde{r}$. It can be seen that the last maximum of $g(\tilde{r})$, which is larger than the standard deviation is between the truncation for 100 and 200 particles. Therefore, $N = 200$ is sufficient to avoid finite size effects. For the gas phase, which is almost ideal, 50 particles are sufficient. Table A1 shows the mean bulk pressure of the LJTS fluid MD simulations obtained in the present work for the metastable region on the liquid and vapour side of the vapour–liquid equilibrium. It also includes some data points for stable states, which are reported here for completeness.

A2. μ − p − T Simulations

Using a modification of the molecular simulation program *ms*2 [58,61], metastable and stable states of the LJTS

Table A1. Thermal properties of the LJTS fluid of stable and metastable states of the liquid and gas. The number in parentheses indicates the statistical uncertainty in the last decimal digit. Stable state points are marked by an asterisk.

	$\tilde{T} = 0.7$		$\tilde{T} = 0.8$		$\tilde{T} = 0.9$		$\tilde{T} = 1.0$	
$\tilde{\rho}$	N	$\tilde{p}$	N	$\tilde{p}$	N	$\tilde{p}$	N	$\tilde{p}$
0.01	864	0.00644(6)*	864	0.007500(49)*	864	0.008548(47)*	864	0.009589(36)*
0.02	864	0.01164(11)	864	0.01397(12)*	864	0.01620(11)*	864	0.01838(11)*
0.04	50	0.0190(7)	864	0.02393(41)	864	0.02879(36)*	864	0.03350(39)*
0.06	50	0.0222(5)	50	0.0313(24)	864	0.0379(7)	864	0.0456(6)*
0.08	-		50	0.0335(43)	50	0.0452(28)	864	0.0551(10)
0.1	-	-	-	-	50	0.0498(45)	864	0.0615(7)
0.15	-	-	-	-	-	-	50	0.0714(13)
0.5	-	-	-	-	-	-	200	0.018(30)
0.55	-	-	-	-	200	−0.118(23)	200	0.042(32)
0.6	-	-	-	-	200	−0.114(8)	864	0.104(13)*
0.65	-	-	200	−0.293(21)	864	−0.015(10)	864	0.253(6)*
0.7	200	−0.500(23)	864	−0.144(15)	864	0.195(14)*	864	0.527(9)*
0.75	864	−0.288(19)	864	0.150(6)*	864	0.582(14)*	864	0.990(20)*
0.8	864	0.145(16)*	864	0.679(15)*	864	1.197(15)*	864	1.690(18)*

fluid are sampled in the $\mu - p$ space for four isotherms ($\tilde{T} = 0.7,\ 0.8,\ 0.9,\ 1.0$). First, MD NpT simulations in the liquid phase are run in which the chemical potential is determined by Widom's test particle method [59]. Then, Monte Carlo (MC) μVT simulations of the vapour phase are carried out in which the pressure is determined. For these μVT simulations the chemical potential calculated in the NpT simulations is used as an input parameter. The pressures of the gas phase and the liquid phase are usually not identical (cf. Figure 5)

The NpT simulations are performed with 1372 particles using 6860 test particles every time step. The simulation time step is $\Delta\tilde{t} = 0.004$. 2000 NVT equilibration time steps and 8000 NpT equilibration time steps are carried out before sampling. The production run is performed for 300000 time steps. The μVT simulations consists of 10000 MC loops for equilibration whereas the production run took 100000 MC loops. Andersen's barostat [60] is used for the NpT simulations. The temperature is kept constant with velocity scaling for both runs. Results are given in Table A2.

A3. Reduced units

The units used in this paper are given in Table A3.

Table A2. Results of the *NpT* and μVT simulations of the LJTS fluid in the stable and metastable region. Stable state points are marked by an asterisk and VLE points are marked with a plus sign. The number in parentheses indicates the statistical uncertainty in the last decimal digit.

	Liquid *NpT* simulations		Vapour μVT simulations
$\tilde{T}$	$\tilde{p}^{\mathrm{l}}$	$\tilde{\mu}$	$\tilde{p}^{\mathrm{v}}$
0.7	0.55001(7)*	−4.102(22)	-
	0.45000(8)*	−4.238(18)	-
	0.35001(8)*	−4.426(19)	0.009946(23)
	0.24999(8)*	−4.570(15)	0.008337(12)
	0.14999(8)*	−4.762(13)	0.006685(9)
	0.04999(7)*	−4.954(10)	0.005399(6)
	0.0048(5)$^{+}$	−5.0522(3)$^{+}$	0.0048(5)$^{+}$
	−0.05000(8)	−5.115(10)	0.004506(6)*
	−0.15000(7)	−5.307(9)	0.0036796(31)*
	−0.24999(7)	−5.494(7)	0.0030185(27)*
	−0.35000(8)	−5.689(6)	0.0024556(23)*
	−0.45000(7)	−5.894(6)	0.0019879(16)*
0.8	0.40001(8)*	−3.542(7)	-
	0.30000(9)*	−3.706(7)	-
	0.19998(8)*	−3.852(7)	-
	0.10002(9)*	−4.025(6)	0.017858(41)
	0.05000(8)*	−4.1101(45)	0.016038(39)
	0.01433(8)$^{+}$	−4.1745(6)$^{+}$	0.01433(8)$^{+}$
	−0.05001(9)	−4.285(5)	0.012875(23)*
	−0.09999(8)	−4.3719(41)	0.011624(14)*
	−0.15000(9)	−4.4629(38)	0.010449(14)*
	−0.20001(8)	−4.5471(48)	0.009494(13)*
0.9	0.20999(8)*	−3.2697(41)	-
	0.16999(8)*	−3.3332(36)	-
	0.12998(8)*	−3.3953(28)	-
	0.09000(8)*	−3.4600(34)	0.03491(13)
	0.0349(2)$^{+}$	−3.548(6)$^{+}$	0.0349(2)$^{+}$
	0.01001(9)	−3.5945(26)	0.03258(13)*
	−0.00999(9)	−3.6297(27)	0.03077(9)*
	−0.03001(9)	−3.6616(27)	0.02933(11)*
	−0.05001(9)	−3.7001(26)	0.02768(6)*
	−0.06998(9)	−3.7309(28)	0.02733(8)*
1.0	0.11000(9)*	−3.0152(23)	-
	0.09999(9)*	−3.0319(23)	-
	0.08998(10)*	−3.0449(19)	-
	0.07998(10)*	−3.0644(27)	-
	0.07000(9)*	−3.0798(18)	-
	0.06118(10)	−3.0982(20)	-
	0.05500(10)	−3.1072(20)	-
	0.05000(8)	−3.1177(16)	-
	0.04499(10)	−3.1240(18)	-
	0.04001(9)	−3.1334(22)	-
	0.03499(9)	−3.1435(28)	-

Table A3. Definitions of physical properties in reduced units.

Length	$\tilde{z} = z/\sigma$
Area	$\tilde{S} = S/\sigma^2$
Temperature	
Density	$\tilde{\rho} = \rho\sigma^3$
Pressure	
Surface tension	
Time	
Free energy per particle	
Free energy	
Potential energy	
Influence parameter	